A HYBRID RANS-LES SOLUTION OF THE FLOW AROUND AN AIRFOIL-FLAP CONFIGURATION

Qinyin Zhang, Wolfgang Schröder, Matthias Meinke
Institute of Aerodynamics,
RWTH Aachen University
Wüllnerstr. zw. 5 u. 7, D-52062 Aachen, Germany
q.zhang@aia.rwth-aachen.de

ABSTRACT

High Reynolds number flows are particularly challenging problems for large eddy simulations (LES). This is due to the resolution of small-scale structures in the thin and often transitional boundary layers. For airfoil flow in high-lift configuration, in which separation regions exist, the range and the disparity of the scales are enormous. For this reason, the prediction of high Reynolds number airfoil flow with LES, which cover the whole configuration, still requires huge computer resources. A hybrid zonal RANS-LES method for the flow over an airfoil in high-lift configuration at $Re_c = 1.0 \cdot 10^6$ is presented in this paper. The solution is obtained by first carrying out a 2D RANS solution, from which boundary conditions are formulated for a zonal domain for the LES, which comprises the flap and only a part of the main airfoil. The turbulent boundary layers at the inflow region of the LES domain on both sides of the main airfoil are generated by using controlled forcing terms which use the turbulent shear stress profiles obtained from the RANS solution. A comparison with an LES for the full domain and also experimental data shows good agreement of all results. Compared to the LES for the full domain the computational effort for the hybrid RANS-LES solution is reduced to about 50%.

INTRODUCTION

The prediction of high Reynolds number flow based on large-eddy simulations (LES) still requires enormous computer resources. Since the flow regions, which require an LES to obtain more accurate results, e.g. for areas with separated flow, are often relatively small, the application of hybrid RANS-LES solutions should reduce the required computational time considerably. A major problem for such an approach occurs, where a turbulent flow from the RANS region enters the LES zone. In that case the time averaged flow variables have to be transformed into spatially filtered variables, which should contain the most energetic part of the turbulent spectrum.

For the zonal LES of the airfoil-flap configuration presented in this paper we use overlapping RANS-LES domains. At the inflow boundaries of the LES domain, controlled source terms, which depend on the local turbulent shear stress profiles of the LES and which are based on the RANS solution, are used to generate a turbulent inflow (Spille and Kaltenbach, 2001). Currently, the RANS solution is only used to determine the boundary conditions for the zonal LES, i.e., the results of the LES solution do not influence the RANS solution.

NUMERICAL METHOD

LES

For the LES the filtered Navier-Stokes equations for three-dimensional compressible flow are solved. The applied block-structured flow solver is based on a vertex centered finite-volume technique, where the equations are implicitly filtered by a top-hat filter. The filtered equations with mass-weighted variables written in nondimensionalized vector form for generalized coordinates $\xi_{i=1,2,3}$ are given by:

$$\frac{\partial \boldsymbol{Q}}{\partial t} + \frac{\partial \boldsymbol{F}_{a,i}}{\partial \xi_i} = \frac{\partial \boldsymbol{F}_{v,i}}{\partial \xi_i} \,. \tag{1}$$

Due to the nonlinearity of the governing equations, the numerical scheme for the spatial discretization have a strong impact on the solution, and therefore need to be selected carefully. It has been shown that a mixed central-upwind AUSM (Advective Upstream Splitting Method) scheme with low numerical dissipation is appropriate for the discretization of the convective fluxes (Meinke et al., 2002). The idea of the AUSM method was introduced by Liou and Steffen Jr. (1993), who split the inviscid fluxes $\boldsymbol{F}_a$ into a convective $\boldsymbol{F}_a^C$ and a pressure part $\boldsymbol{F}_a^P$. After inserting the local sound speed c, the convective part is reformulated with a Mach number weighted interpolation

$$\begin{aligned} \hat{\boldsymbol{F}}_a^c = \; & \tfrac{1}{2} \Big[(Ma_+ + Ma_-) \, (\boldsymbol{f}_-^c + \boldsymbol{f}_+^c) \\ & + |Ma_+ + Ma_-| \, (\boldsymbol{f}_-^c - \boldsymbol{f}_+^c) \Big] \,. \end{aligned} \tag{2}$$

The fluxes $\boldsymbol{f}_\pm^c$ and the Mach number $Ma_\pm$ are determined by interpolated primitive variables on the left $(-)$ and right $(+)$ cell faces. The pressure part of the inviscid term is calculated with a split form, where the pressure value is formulated by a Mach number weighted interpolation

$$p_\pm = p_\pm \, (\frac{1}{2} \pm \chi \, Ma_\pm) \quad . \tag{3}$$

Investigations have shown that the parameter χ, which represents the rate of change of the pressure ratio with respect to the local Mach number, has a strong influence on the numerical dissipation of the scheme. A central splitting with $\chi = 0$ gives clearly less numerical dissipation and is well suited for performing LES. The viscous terms are discretized by a central scheme of second-order accuracy. The temporal integration is done by a 5-step-Runge-Kutta method, where the coefficients are optimized for maximum stability. These discretization schemes result in an overall approximation of second-order accuracy in space and time. For a detailed description of the method the reader is referred to Meinke et al. (2002).

Through the filtering operation applied to the Navier-Stokes equations, the turbulent motion is separated into a resolved and an unresolved part. The primary influence of the unresolved motion on the resolved scales is to remove turbulent energy from them. Several SGS modeling approaches, such as the Smagorinsky SGS model, its dynamic variant, and the ADM (Approximated Deconvolution Method) have been implemented into the current flow solver. Experience has shown that convincing results are already obtained without any SGS model. In many cases, the Monotone Integrated LES (MILES) approach yielded better results than calculations with activated SGS modeling. This is due to the fact that the truncation error of the spatial discretization can provide a mechanism by which turbulent energy is dissipated and as such serves as an SGS model. The theoretical basis of MILES is rigorously discussed by Fureby and Grinstein (1999), and excellent results have been obtained in numerous simulations of internal and external turbulent flows. For the current LES, we use the MILES approach.

RANS

The RANS simulation is based on the solution of the time-averaged Navier-Stokes equations. Since the time-averaged equations are not closed, a turbulence model should relate the unknowns to the mean flow variables and closes the system of equations. In the present work, the Spalart Allmaras turbulence model (Spalart and Allmaras, 1992) was chosen for the RANS simulation on the full mesh. The results of the RANS simulation are then used for the hybrid RANS-LES coupling in the transfer zone and for the turbulent inflow generation at the inlet of the zonal LES for the airfoil-flap configuration.

Sponge Layer

On the farfield boundary of the full LES domain and on the outer boundary of the zonal LES region, special treatment is needed to reduce spurious numerical reflections. An efficient method to reduce disturbances is to introduce a buffer domain, the so-called sponge layer, near the boundary, in which additional local damping is applied to reduce fluctuations. A source term vector, which depends on the deviation of the instantaneous conservative flow variables from the turbulent steady state values is added to the right-hand side of the Navier-Stokes equations. This method has been used successfully in various simulations to reduce numerical reflections.

COMPUTATIONAL SETUP

Airfoil-flap configuration

The airfoil-flap geometry for the current study is shown in Fig. 1 together with the locations of the velocity measurements. The airfoil-flap geometry was defined within the framework of the German national project SWING+ (Würz et al., 2002). The freestream Mach number is Ma_∞=0.12, and the Reynolds number based on the chord length is $Re_c = 1.0 \times 10^6$. The numerical simulations are carried out for an angle of attack at $\alpha = 0°$.

The full LES was performed for the whole airfoil-flap configuration with the far-field boundary placed at approximately 13 $\sim$ 15 chord lengths away from the airfoil surfaces. The spanwise extension is set to be 1.28% of the chord length. This length approximately corresponds to the radius of the eddies which appear in the flap cove due to the separation from the sharp cove lip on the downside of the main airfoil. The computational grid for the full LES comprises 12.7 million cell volumes. The wall is resolved with a smallest wall distance of $\Delta y^+_{min} \approx 2$. The stream- and spanwise resolution are $\Delta x^+ = 150 \sim 200$ and $\Delta z^+ \approx 20$, respectively. A 2D RANS computations was also carried out on the above described mesh.

To show the validity of the zonal LES concept, the influence of the mesh should be minimized. For this reason, the zonal LES is performed on a mesh, which is identical to an inner part of the full LES mesh. The boundaries of the zonal mesh are marked in Fig. 2 and the mesh properties are summarized in Tab. 1. The indicated zones "I" and "II" are the zones in which the turbulent inflow will be generated. The 3D zonal LES simulation is carried out in the zone "III". The inlet planes for the zonal LES are placed right ahead of the trailing edges, since the time averaged values of the turbulent boundary layers on the upper and lower side of the airfoil are considered to be predictable by the RANS approach. The unsteady characteristics of the turbulent boundary layers at the inlet of the zonal mesh are generated by using the forcing term technique that will be explained later. Test cases have shown that the turbulent flow needs a short development distance to reach the correct turbulence characteristics. For this reason, the inflow generation zones "I" and "II" are chosen to have lengths of 15 $\sim$ 20 δ and heights of 3 $\sim$ 5 δ, according to the boundary layer thickness δ of the upper and lower airfoil surfaces, respectively.

Table 1: Grid distribution for the full and zonal LESs of the SWING+ Airfoil.

	$N_x \times N_y$	N_z	Cell Number
Full Mesh	311,238	41	12,760,758
Zonal Mesh	181,470	41	7,440,270

A 2D RANS computation is carried out on the full mesh previous to the zonal LES to define the transfer zones between the zonal and the full mesh. The Reynolds shear stress profiles on some discrete locations, which are obtained from the RANS simulation, are used for the turbulent inflow generation in the zones "I" and "II".

For this airfoil-flap configuration, the main unsteady flow phenomena are the turbulent shear layer behind the trailing edge of the main airfoil, the separation in the flap cove, and the highly unsteady flow field around the flap with a small separation bubble above the suction side of the flap close at the trailing edge. These flow regions are completely covered by the zonal mesh. The RANS zone contains the regions with attached boundary layers, in which standard turbulence models are expected to predict accurate solutions. The qualitative higher-valued but also much more expensive LES method, which is capable to resolve highly unsteady turbulent flow fields, is applied in non-equilibrium and separated flow regions. This concept is considered to be able to successfully combine the advantages of the RANS and LES methods. This is the main objective of the current study.

Boundary conditions

An adiabatic no-slip wall is imposed on the airfoil and flap surfaces. For the spanwise direction, periodic boundary conditions are used. To avoid spurious waves, non-reflecting boundary conditions are applied in conjunction with a sponge layer on the outer boundaries for the full LES simulation. For the interface region between the zonal LES domain (zones "I", "II" , and "III") and the full mesh, a sponge layer technique is used to assure a smooth transfer of the flow variables from the LES to the RANS zone. At the inlet of the zonal LES simulation, a special turbulent inflow generation technique is used. It will be explained in the following section.

TURBULENT INFLOW GENERATION

The method proposed by Spille and Kaltenbach (2001) uses a number of control planes at discrete positions to amplify the wall-normal velocity fluctuations v', so that a given Reynolds shear stress (RSS) profile $\langle u'v'\rangle^*$ can be matched. A body force is added to the wall-normal momentum equation on control planes

$$\frac{\partial}{\partial t}(\bar{\rho}\tilde{u_i}) + \frac{\partial}{\partial x_j}(\bar{\rho}\tilde{u}_i\tilde{u}_j) = -\frac{\partial \bar{p}}{\partial x_i} + \frac{\partial \bar{\tau}_{ij}}{\partial x_j} + \frac{\partial \tau_{ij}^{SGS}}{\partial x_j} + \delta_{i2} f \quad . \tag{4}$$

In the work of Keating et al. (2004) this method has shown promising results and produced correct turbulent statistics after a relatively short distance. For a detailed discussion of various turbulent inflow conditions we refer to the work by Keating et al. (2004) who reviewed and compared several LES inflow conditions in detail.

The approach operates similar to a closed-loop control system. The difference between the current and the target RSS-profile is the error function $e(y,t)$, which acts as the input parameter for the control system

$$e(y,t) = \langle u'v'\rangle^*(x_i, y) - \langle u'v'\rangle^{z,t}(x_i, y, t) \quad . \tag{5}$$

The term $\langle u'v'\rangle^*(x_i, y)$ is the target RSS at the $i-$th control plane at $x = x_i$, and the term $\langle u'v'\rangle^{z,t}(x_i, y, t)$ is the calculated RSS on the $i-$th control plane at the time t which has been averaged over the spanwise direction and in time. The spatial and temporal averaging are denoted by the superscripts z and t, respectively. The calculation of the fluctuations u_i' and the building of the time averaged shear stress $\langle u'v'\rangle$ is based on the running average of the mean flow velocity field by using an exponential window in time.

The amplitude of the introduced force term is controlled by the error function according to

$$r(y,t) = \alpha\, e(y,t) + \beta \int_0^t e(y,t')dt' \quad . \tag{6}$$

The forcing term, which should be added to the right hand side of the wall-normal momentum equation, reads

$$f(x_i, y, z, t) = r(y,t)[u(x_i, y, z, t) - \langle u\rangle^{z,t}(x_i, y)] \quad . \tag{7}$$

The constants α and β define the proportional and integral behavior of the PI-controller respectively and should be chosen such that the error signal can be reduced sufficiently in a short time and no instabilities are generated. The parameters are solver and case dependent. Good results were obtained with the control parameters $\alpha = 40$ and $\beta = 0.25$.

For validation, a spatially developing plane channel flow was simulated for a viscous Reynolds number of $Re_\tau = 590$. The results of the simulation were compared with the DNS results of Moser et al. (1999). In the case of a developing channel flow, the turbulent flow needs a certain length in the streamwise direction to become fully developed. Therefore a channel length of $8\pi h$ is used to assure that this developing process is captured by the simulation. The grid resolution for the channel simulation was set with $\Delta x^+ = 24.4$, $\Delta y^+_{min} = 2$, $\Delta y^+_{max} = 21.3$, and $\Delta z^+ = 20.1$. The computational mesh comprises about 8.2 million cells. No-slip and adiabatic wall condition are used for the channel walls. At the exit, an extrapolation boundary condition is applied. On the inlet plane of the channel, an analytical velocity profile without turbulent fluctuations is prescribed according to the logarithmic law of the wall.

In four planes (x_1/h=0.91, x_2/h=1.94, x_3/h=2.85, and x_4/h=3.99) downstream from the channel inlet (x/h=0), controlled source terms are added to the momentum equation in the wall normal direction according to the equations from Eq. 4 to Eq. 7. The locations of the control planes and the contours of the turbulent kinetic energy (TKE) $k = \frac{1}{2}\langle u_i'u_i'\rangle$ at a wall distance of $y/h = 0.026$ are shown in Fig. 3. The TKE value is zero until the first control plane is reached by the flow. Immediately after passing the first control plane at $x/h = 0.91$, TKE begins to increase and longitudinal turbulent eddies appear. The effectiveness of the Spille-Kaltenbach controlled forcing method can be clearly seen in Figs. 4 and 5, where the streamwise development of the TKE and the RSS profiles are shown by plotting the curves in several streamwise positions. Shortly downstream of the 4-th control plane, the TKE reaches a quasi-developed state, which is in very good agreement with the DNS results. A similar behavior is observed for the RSS curves.

RESULTS

In the current study, LES and RANS computations were conducted on the full mesh for the airfoil-flap configuration, while a hybrid RANS/LES simulation was performed on the zonal mesh. In the following, the full LES results for the airfoil-flap configuration will be presented first. They serve as a reference solution.

The resolution requirements for a resolved LES of wall-bounded flow are usually given by $\Delta x^+ = 50 \sim 100$, $\Delta y^+ = 2$ and $\Delta z^+ = 20$. To fulfill these resolution requirements, a mesh with a total cell number of around 100 million would be needed. Due to limited computer resources, a mesh with reduced resolution was used for the current simulation (Tab. 1). The resolution in the streamwise direction is set to be $\Delta x^+ \approx 200 \sim 300$, while the wall-normal and the spanwise resolutions were kept as required. This was considered to be a good compromise between acceptable computing efforts and resolution requirements. Since in the current case the main purpose to perform the full LES was to generate a reference solution for the comparison with hybrid zonal method, these resolution settings were considered to be sufficient.

If the full LES solution can be considered to be fully developed, a time window of $\Delta T = 5.0\, c/u_\infty$ was used for the temporal averaging process, then the solution was further spatially averaged in the spanwise direction. The time and spanwise averaged data were then compared with the data gathered in experiments performed by IAG Stuttgart (Würz et al., 2002). The comparison of the numerical and the experimental results showed a very good agreement in the pressure coefficient distribution $C_p(x)$ (Fig. 9). Nevertheless, the size of the separation bubble, which is characterized by the plateau in the C_p distribution, was not given exactly by the current simulation. The time and spanwise averaged velocity profiles are compared with experimental data in Fig. 10. The overall agreement of the velocity profiles is considered to be qualitatively satisfactory. For a wall-bounded LES, if the mesh resolution is not fine enough, the streamwise velocity fluctuations can not be easily redistributed into the wall-normal direction. A result of this phenomenon is that the velocity profile tends to be over predicted in the streamwise direction, which can be seen at the velocity profile at the position "A" in Fig. 10. It will be shown later that the use of the zonal LES concept with artificially excited turbulent inflow, this deficiency can be remedied partly. It was further observed in the experiments that the flow on the airfoil lower side undergo a free transition at 68% chord length, and a laminar separation bubble appears right before the flap cove lip at $x/h = 0.70$. To avoid this phenomenon the flow was tripped at the position $x/c = 0.5$ later during the experimental velocity measurements (Würz et al., 2002). The velocity profile of the full LES at the position "E" ($x/c = 0.695$) corroborate the observations of the free transition case.

At the first step of the zonal simulation, a RANS calculation was conducted on the 2D full mesh with $311,238$ mesh points with the Spalart-Allmaras turbulence model. The used model is calibrated for the flow around airfoils at high Reynolds numbers. The computed velocity profiles and the pressure coefficients from the RANS simulation are presented in Fig. 6(a) and 6(b). The velocity profiles show very good agreement with the experimental results and the boundary layer thicknesses were predicted correctly. The small separation bubble at the end of the flap was computed exactly, this can be seen in the plateau of the $C_p(x)$ distribution near the end of the flap. For the RANS approach there are many possibilities in tuning the model constants. It is not surprising that for the standard airfoil case good time-mean results can be reproduced correctly. Nevertheless, no information about the highly unsteady three-dimensional flow field inside the flap cove can be expected from a RANS simulation. In order to reveal unsteady flow field details, a zonal LES is performed subsequently.

The zonal LES is conducted for the domain shown in Fig. 2. The Spille-Kaltenbach method is applied to the zones "I" and "II", such that at the inlet of the zonal LES domain (zone "III") developed turbulent boundary layers are present. By passing the control planes, turbulent structures begin to appear, similar to the channel case. After a development length of about 0.2 chord on the upper and lower airfoil surfaces, the turbulent boundary layers are fully developed. Tests have shown that the development to the fully turbulent boundary layer is influenced by the grid resolution, i.e., a smaller spatial steps in the streamwise direction leads to a faster fully developed turbulent boundary layer. This means, the purpose of using the inflow generation zones to provide turbulent fluctuations in equilibrium with the mean flow at the inlet of the zonal simulation is fulfilled.

The resolved turbulent coherent structures in the full and zonal simulations are visualized by the λ_2 criterion and shown in Figs. 7 and 8. The turbulent structures display the extremely complex flow dynamics in the flap cove. Comparison between the full and the zonal solution shows qualitatively very similar results. This is due to the fact that the main unsteady flow physics is completely covered by the zonal domain, which in turn justifies the zonal concept applied to this case.

The time and spanwise averaged pressure coefficients and velocity profiles are compared with full LES results and experimental data in Fig. 9 and Fig. 10. For the pressure coefficient, deviations can be seen at the beginning of the inflow generation zones "I" and "II". This is caused by the source terms added to the momentum equation on the locations of the control planes that leads to unphysical pressure variations. Shortly downstream, the distribution shows an almost exact match to the full LES results. A small recirculation region near the end of the flap can be seen in the λ_2 iso-surfaces in Figs. 7 and 8. However, this fact is not reflected in the $C_p(x)$ distributions of the LESs.

As mentioned before, the velocity profile at the position "A" is overpredicted by the full LES in the outer part of the boundary layer due to insufficient momentum exchange in the wall normal direction, which is also a direct consequence of the underresolved mesh. Using the Spille-Kaltenbach method, an artificial and physically correct turbulent boundary layer is generated at the inlet of the zonal mesh. The contained fluctuations in the momentum exchange leads to a better redistribution of the TKE from the streamwise direction to the wall-normal direction. This reduces the wall parallel and increases the normal component of the velocity, such that a better agreement with experimental data is achieved. In the free transition case the laminar flow laminar separates at the position "E", which can also be seen in the full LES velocity profile. Since the velocity measurements were performed with tripped turbulent flow at $x/c = 0.5$. A turbulent velocity profile is given by the experiment at "E". With the velocity fluctuations contained in the boundary layer generated in the zone "II" of the zonal simulation, the flow is now able to overcome the positive pressure gradient, and the velocity profile of the zonal LES gives a better match with the experimental data.

Since there are no RMS-profiles provided by the experiments, the TKE contour of the full and zonal simulations are compared in Fig. 11. As can be expected from the previous discussions, the fluctuation statistics are also in good agreement with each other.

CONCLUSIONS

A hybrid RANS-LES solution has been presented for an airfoil-flap configuration. The findings show that the computational effort can be easily reduced by nearly 50%, if a zonal concept is applied. The flow field was divided into two zones and a 2D RANS simulation was performed in the zone in which only attached boundary layers exist (i.e. surface of the main airfoil) and therefore RANS-models are considered to be well applicable. In zones where massively separated flow regions exist (flap cove) and highly unsteady turbulent mixing processes are present (flow field around the flap), the LES was carried out. At the outer interface boundaries between both zones a sponge layer technique drives the flow variables towards those extracted from the RANS results. A turbulent inflow generation technique according to Spille and Kaltenbach (2001) was tested for a turbulent channel flow at $Re_\tau = 590$ and then applied at the inlet of the zonal simulation to generate realistic turbulent boundary layers.

The comparison of the zonal results with the full LES and also experimental data shows good agreement with each other. Due to the realistic turbulent boundary layer generated at the inlet zone, the results were improved in some details in comparison to the full LES results. In the next step, the unsteady flow features associated to the noise generation will be studied. Further research is currently carried out for a fully coupled RANS-LES method and also for unsteady RANS solutions.

REFERENCES

Fureby, C. and Grinstein, F.F. 1999. Monotonically integrated large eddy simulation of free shear flows. *AIAA J.*, Vol. 37(5), pp. 544–556.

Keating, A., Piomelli, U., Balaras, E., and Kaltenbach, H.-J. 2004. A priori and a posteriori tests of inflow conditions for LES. *Phys. of Fluids*, Vol. 16, no. 12, pp. 4696–4712.

Liou, M. S. and Steffen Jr., Ch. J. 1993. A new flux splitting scheme. *J. Comp. Phys.*, Vol. 107, pp. 23–39.

Meinke, M., Schröder, W., Krause, E., and Rister, Th. 2002. A comparison of second- and sixth-order methods for large-eddy simulations. *Computers and Fluids*, Vol. 31, pp. 695–718.

Moser, R. D., Kim, J., and Mansour, N. N. 1999. Direct numerical simulation of turbulent channel flow up to Re_τ=590. *Phys. of Fluids*, Vol. 4, no. 11, pp. 943–945.

Spalart, P. R. and Allmaras, S. R. 1992. A one-equation turbulence model for aerodynamic flows. AIAA Pap. 92-0439.

Spille, A. and Kaltenbach, H.-J. 2001. Generation of turbulent inflow data with a prescribed shear-stress profile. Cp, Hermann-Föttinger-Inst., TU Berlin. 3rd AFSOR Conference on DNS and LES, Aug. 5.-9.

Würz, W., Guidati, S., and Herr, S. 2002. Aerodynamische Messungen im Laminarwindkanal im Rahmen des DFG-Forschungsprojektes SWING+ Testfall 2. Inst. für Aerodynamik und Gasdynamik, Universität Stuttgart, 2002.

FIGURES

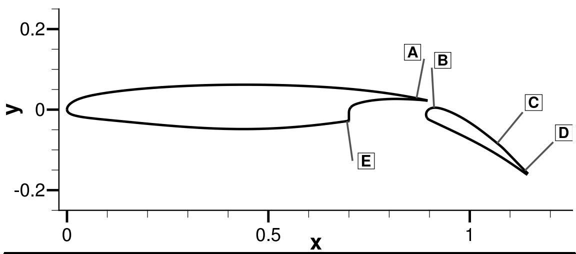

positions	A	B	C	D	E
x/c	0,868	0,910	1,068	1,138	0,695

Figure 1: Airfoil-flap configuration and location of the measurements of the velocity profiles.

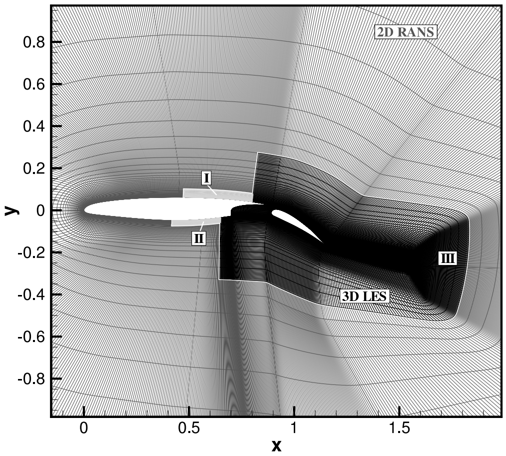

Figure 2: Computational domain of the zonal LES (every second grid points are shown).

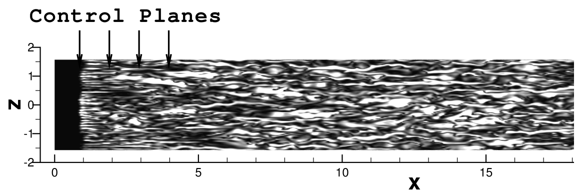

Figure 3: Contours of the turbulent kinetic energy $k = \frac{1}{2}\langle u_i' u_i' \rangle$ at $y/h = 0.026$. The locations of the control planes are indicated by arrows.

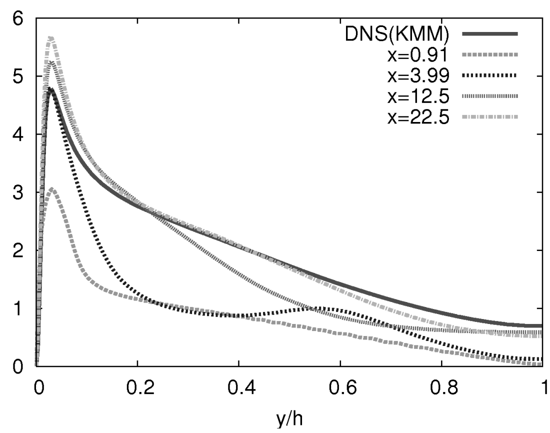

Figure 4: Profiles of the turbulent kinetic energy k at different streamwise locations x/h in comparison to DNS data Moser et al. (1999).

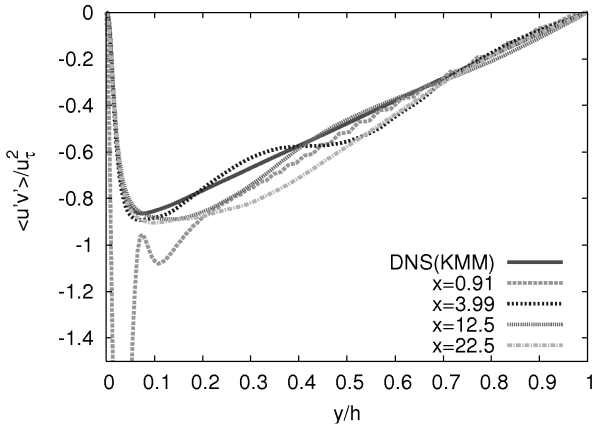

Figure 5: Profiles of the Reynolds shear stress $\langle u'v' \rangle$ at different streamwise locations x/h in comparison to DNS data Moser et al. (1999).

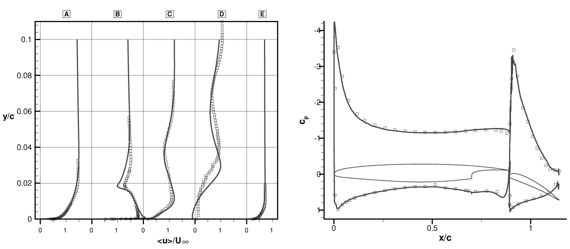

(a) (b)

Figure 6: Results of the RANS simulation: (a) velocity profiles (b) pressure coefficient.

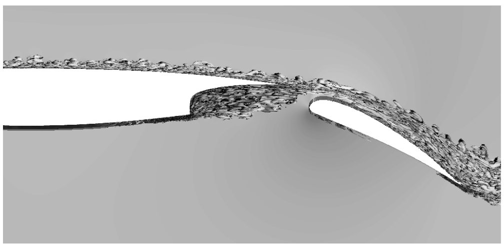

Figure 7: Contours of $\lambda_2 = -0.8$ colored by the local Mach number (Full LES).

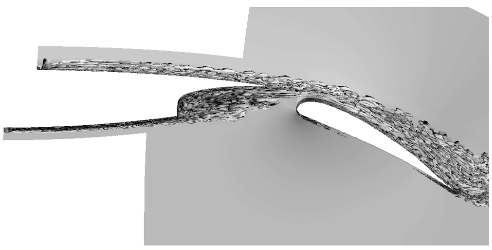

Figure 8: Contours of $\lambda_2 = -0.8$ colored by the local Mach number (Zonal LES).

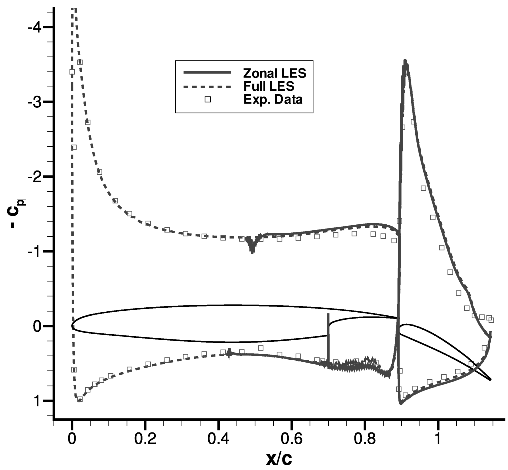

Figure 9: Time and spanwise-averaged pressure coefficient $-C_p(x)$.

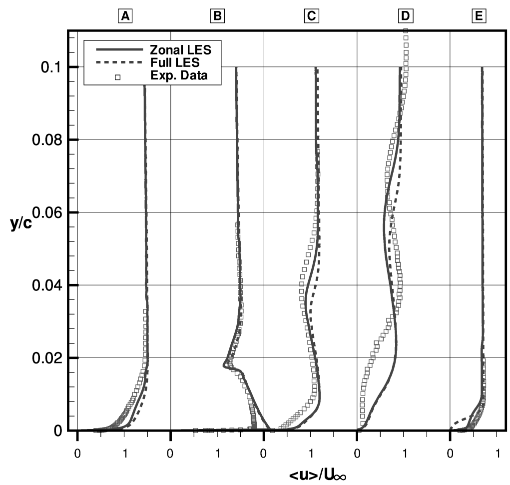

Figure 10: Time and spanwise-averaged wall parallel velocity profiles u/u_∞.

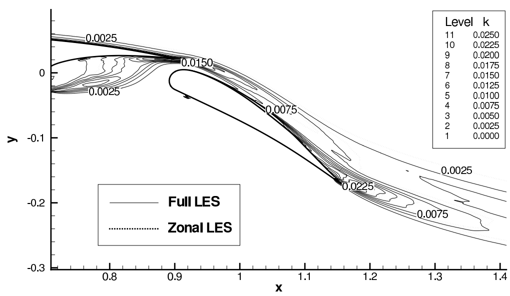

Figure 11: Contours of TKE for full and zonal LES.